

Waveform-based classification of dentate spikes

Rodrigo M.M. Santiago, Vítor Lopes-dos-Santos, Emily A. Aery Jones,
Yadong Huang, David Dupret, Adriano B.L. Tort

Supplementary figures

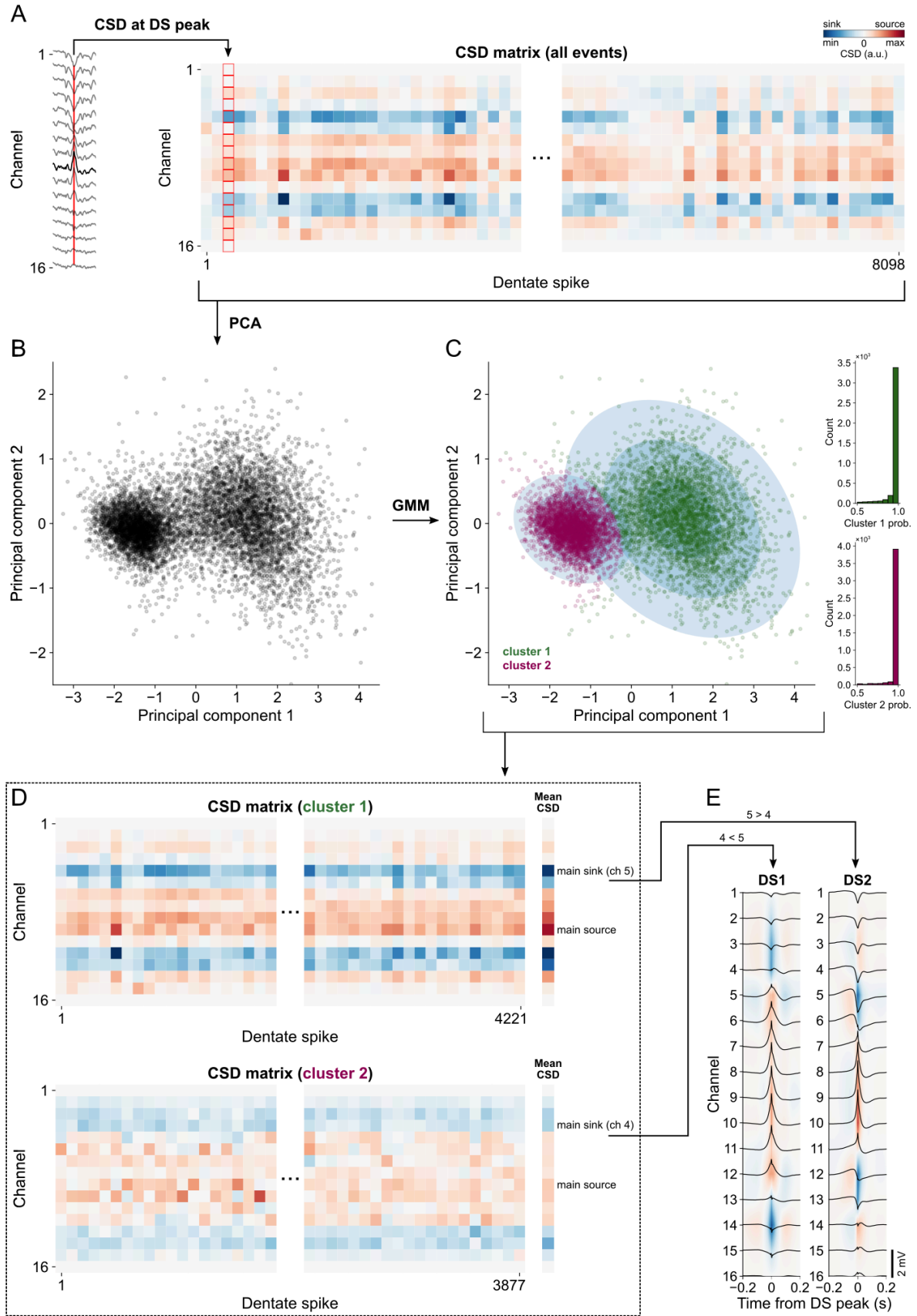
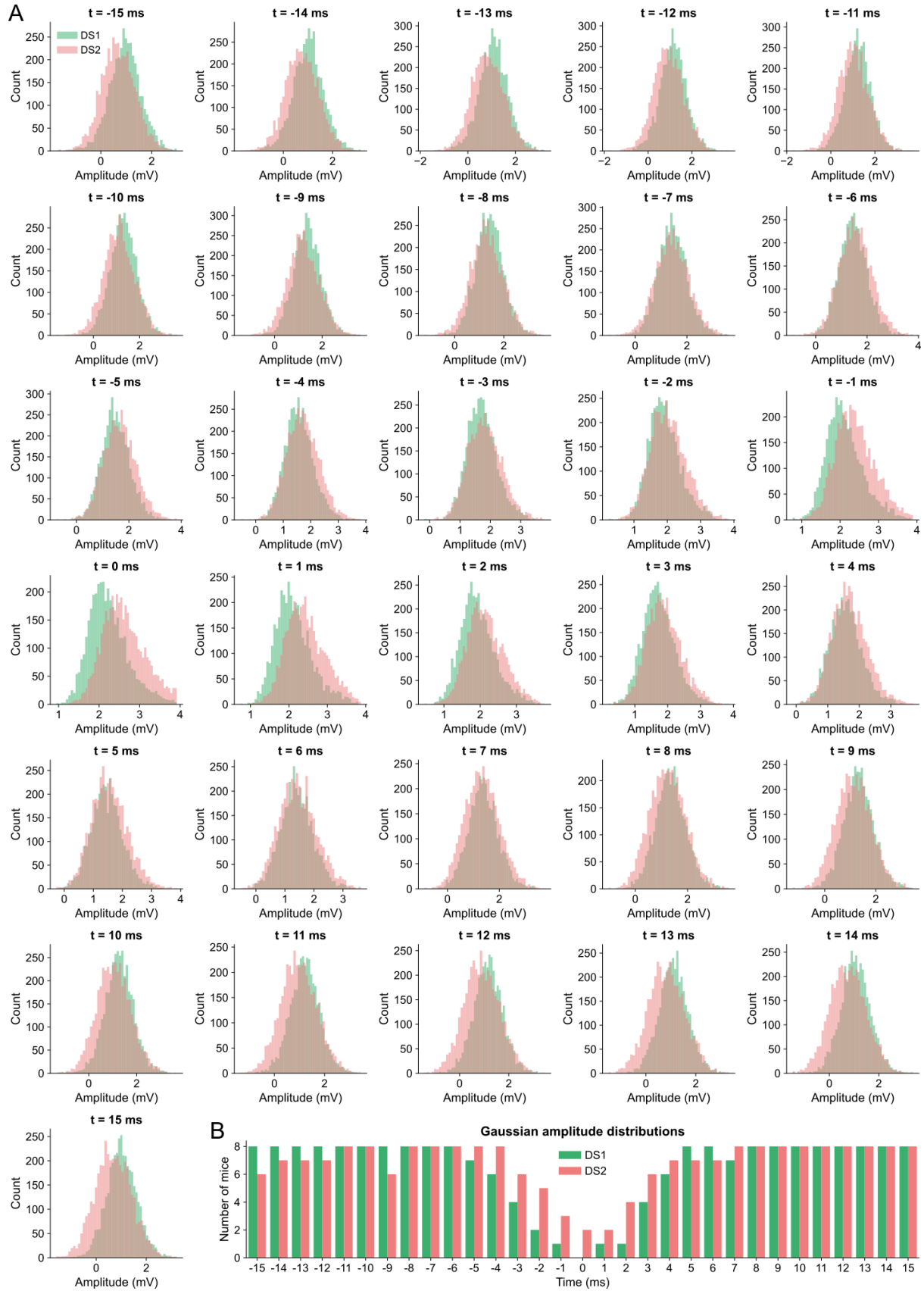


Figure S1. Step by step of the CSDbC method using mouse A DSs.

(A) After DS detection in the hilus channel (bold trace in the left panel), the CSD profiles are calculated at the peak of each event (red line), generating a CSD matrix of events by channels (right panel). (B) The CSD matrix is projected into the two dimensions of greatest covariance by PCA. (C) Events projected into the first principal

component are clustered into two groups by GMM. The ellipses indicate the Gaussian probability distributions of each cluster in three levels. The right panels show a high clustering probability for most events. **(D)** The CSD matrix of each cluster generates a mean CSD profile that indicates the position of the main (most prominent) current sink above the main current source. **(E)** DS type assignment for each cluster based on the positions of the main current sinks. Cluster 2 corresponds to DS1 since the main current sink is located in channel 4, which is above channel 5 (cluster 1 main sink). Panels show the mean CSD profiles and waveforms (black traces) for each DS type. ch: channel; CSD: current source density; DS: dentate spike; DS1: DS type 1; DS2: DS type 2; GMM: Gaussian Mixture Models; PCA: Principal Component Analysis.



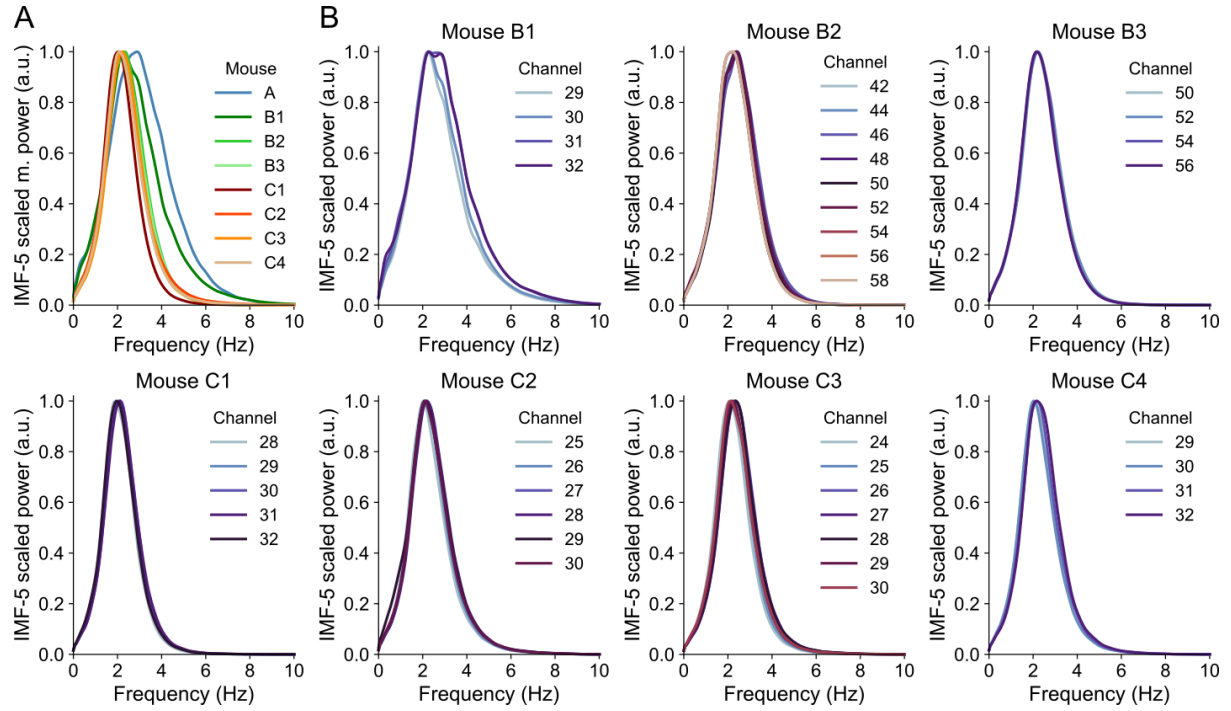


Figure S3. Consistent PSDs of IMF-5 across mice and DG layers.

(A) Normalized mean power of IMF-5 of all mice. Each trace is the mean PSD of one mouse across its relevant channels. (B) Each panel exhibits the normalized IMF-5 PSDs of all relevant channels of each mouse. The panel corresponding to mouse A is shown in the inset of Fig 2A. IMF: intrinsic mode function.

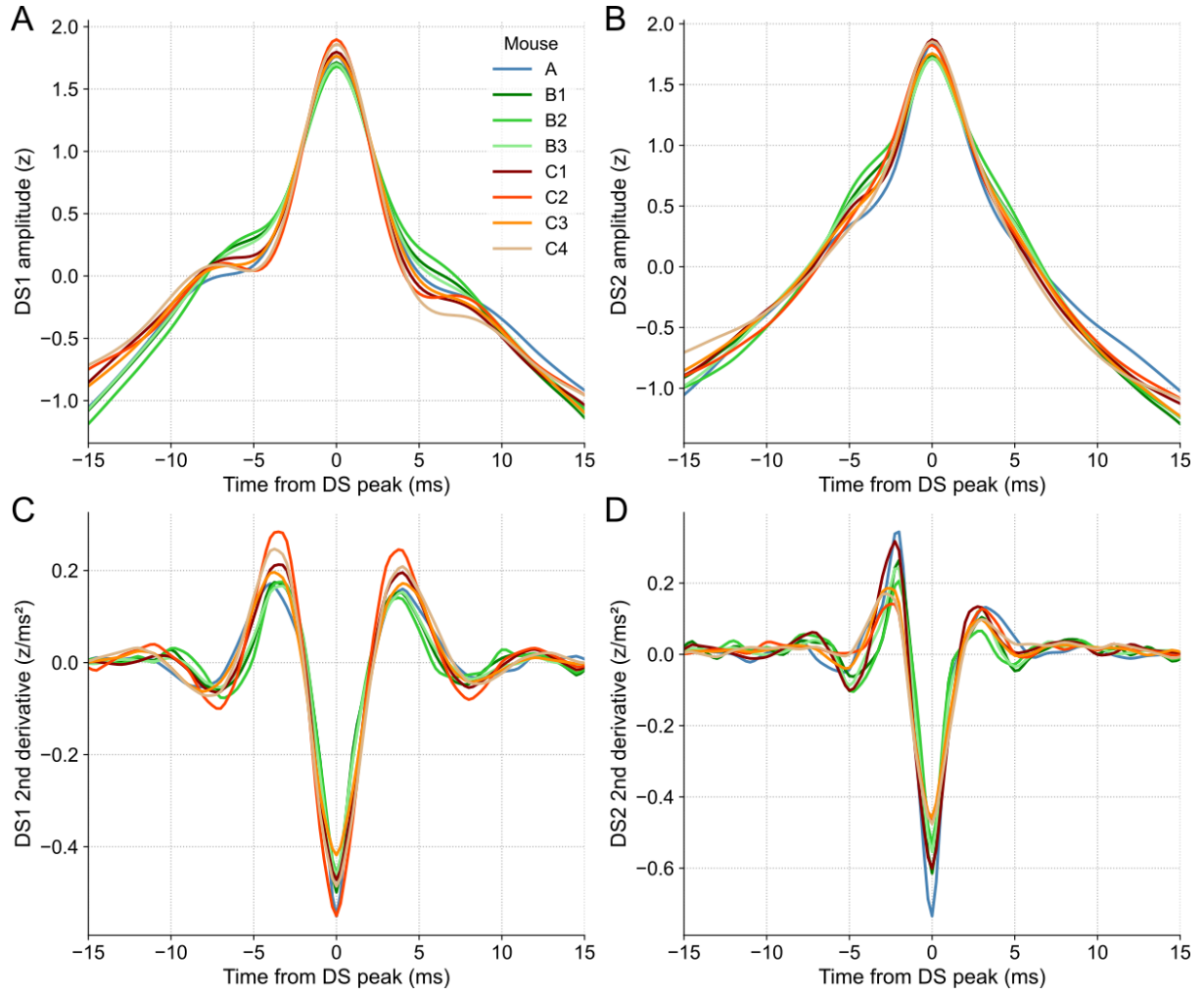


Figure S4. Average waveform dynamics of each DS type of all mice.

(A) Scaled mean waveforms of DS1 detected in the channel that yielded more DSs for all mice. (B) Same as A, but for DS2. (C) The second derivatives of the DS1 waveforms depicted in A. (D) Same as C, but for DS2. DS1: dentate spike type 1; DS2: dentate spike type 2.

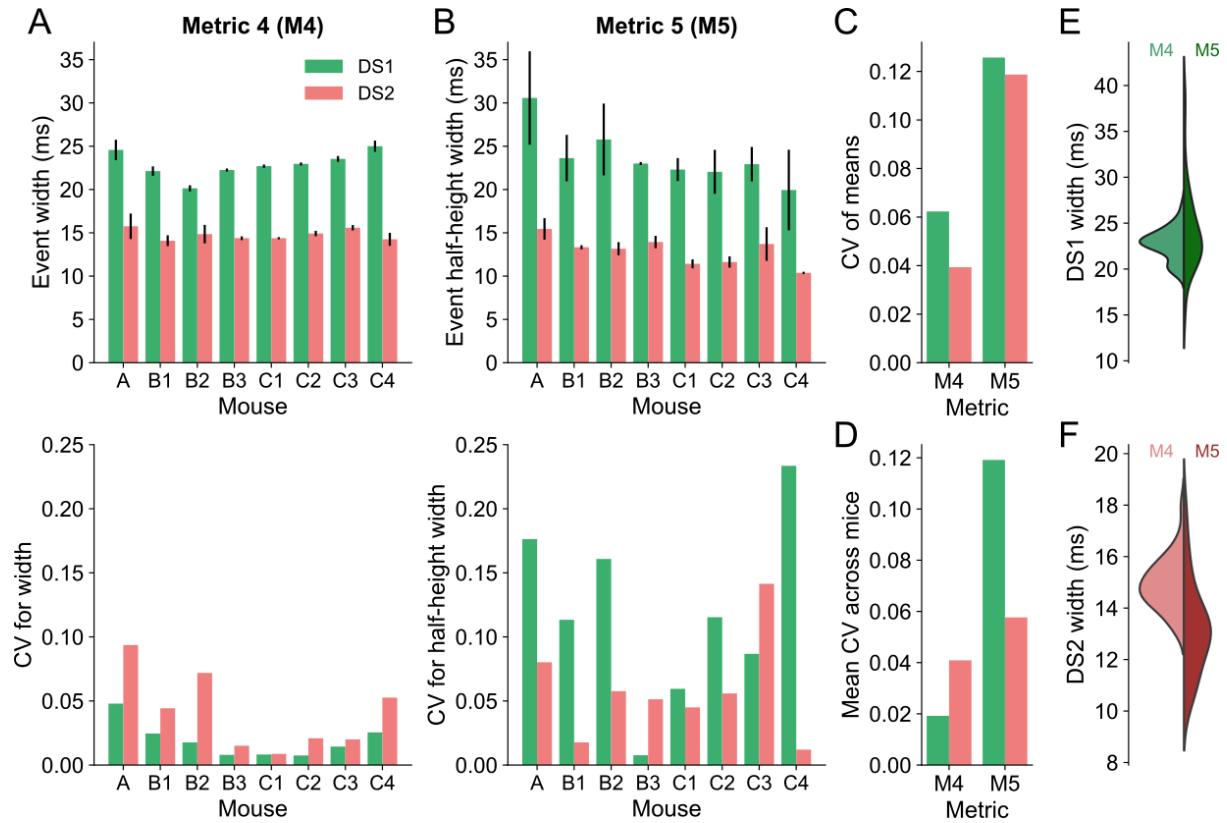


Figure S5. DS width based on waveform dynamics is more stable than width at half height.

(A) The top panel shows the width for each DS type (Metric 4 – M4) across channels for each mouse. Colored bars correspond to the means, and the error bars indicate the standard deviations. The bottom panel shows the coefficient of variation of the corresponding measurements in the panel above. (B) Same as A, but for the width at half-height (Metric 5 – M5). (C) Coefficients of variation of the means of each metric across mice. (D) Mean coefficients of variation of each metric across mice. (E) Distributions of M4 and M5 of DS1 show that M5 is more variable. (F) Same as E, but for DS2. CV: coefficient of variation; DS: dentate spike; DS1: dentate spike type 1; DS2: dentate spike type 2.

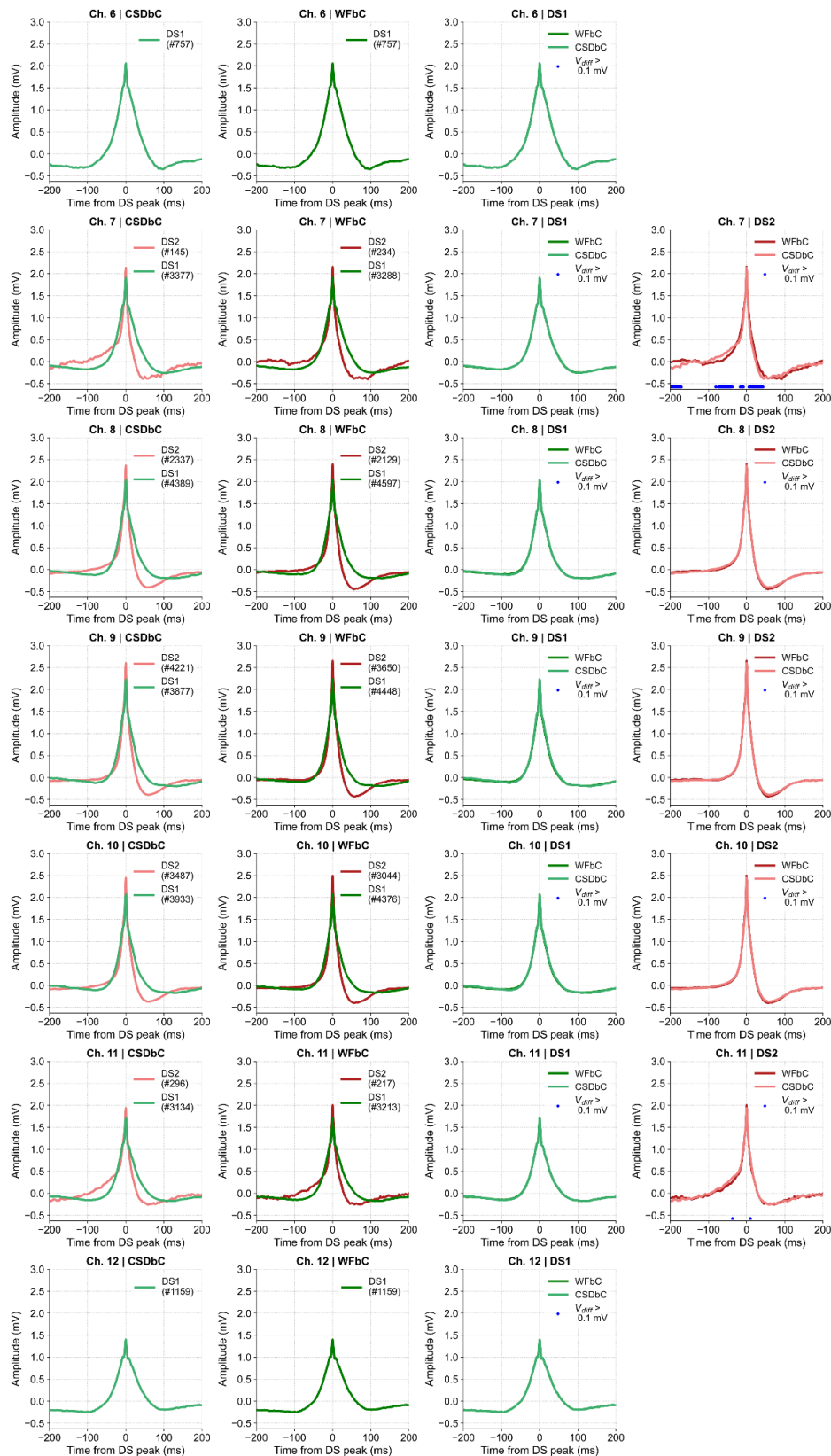


Figure S6. DS waveform comparison between methods for each channel of mouse A.

The panels in the first and second columns show the waveforms of each DS type classified by CSDbC and WFbC respectively. The panels in the third and fourth columns compare the waveforms of DS1 and DS2 respectively. Each line represents the chosen channel for DS detection. CSD: current source density; CSDbC: CSD-based classification; DS: dentate spike; DS1: DS type 1; DS2: DS type 2; WFbC: waveform-based classification.

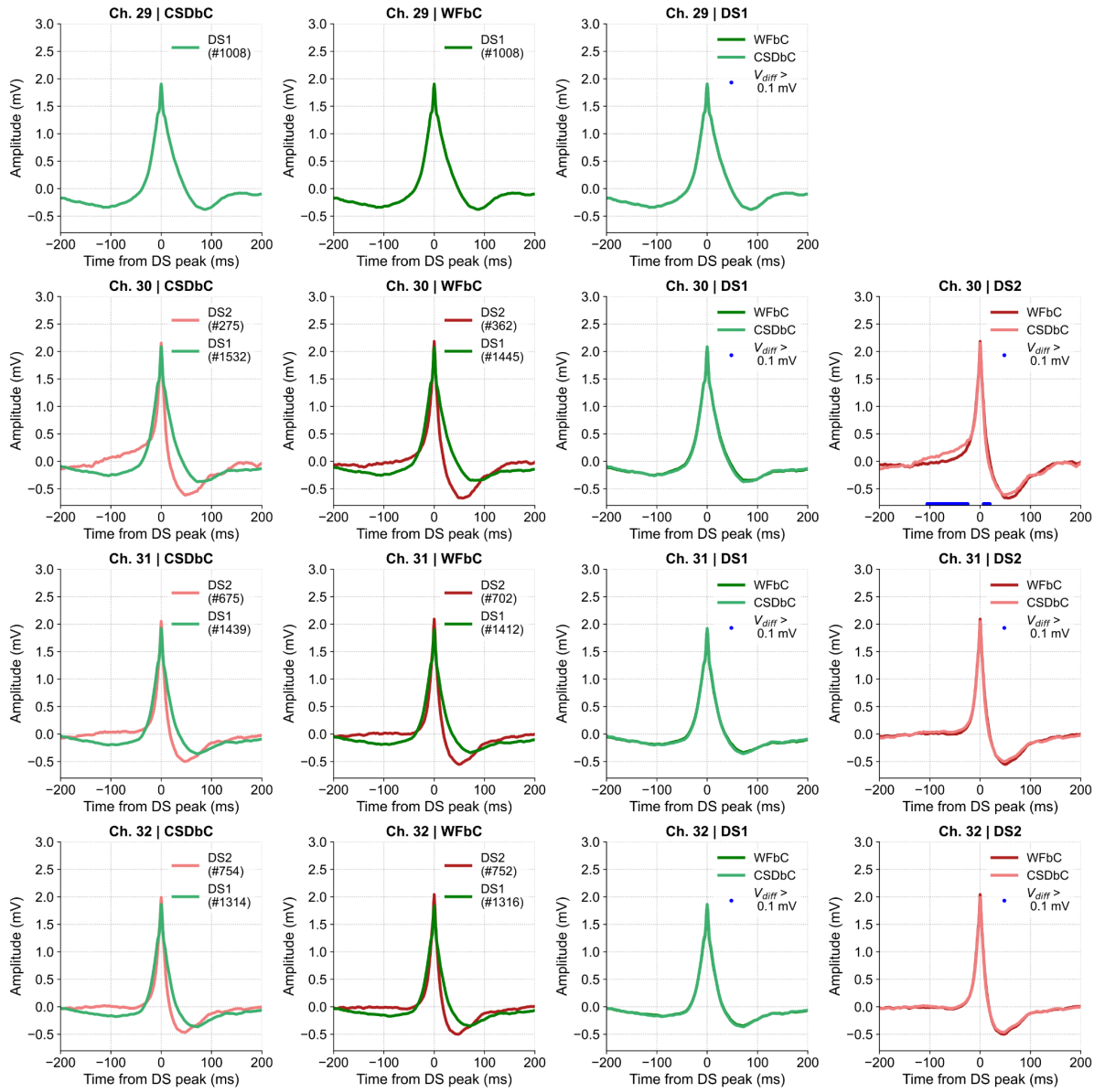


Figure S7. DS waveform comparison between methods for each channel of mouse B1.

The panels in the first and second columns show the waveforms of each DS type classified by CSDbC and WFbC respectively. The panels in the third and fourth columns compare the waveforms of DS1 and DS2 respectively. Each line represents the chosen channel for DS detection. CSD: current source density; CSDbC: CSD-based classification; DS: dentate spike; DS1: DS type 1; DS2: DS type 2; WFbC: waveform-based classification.

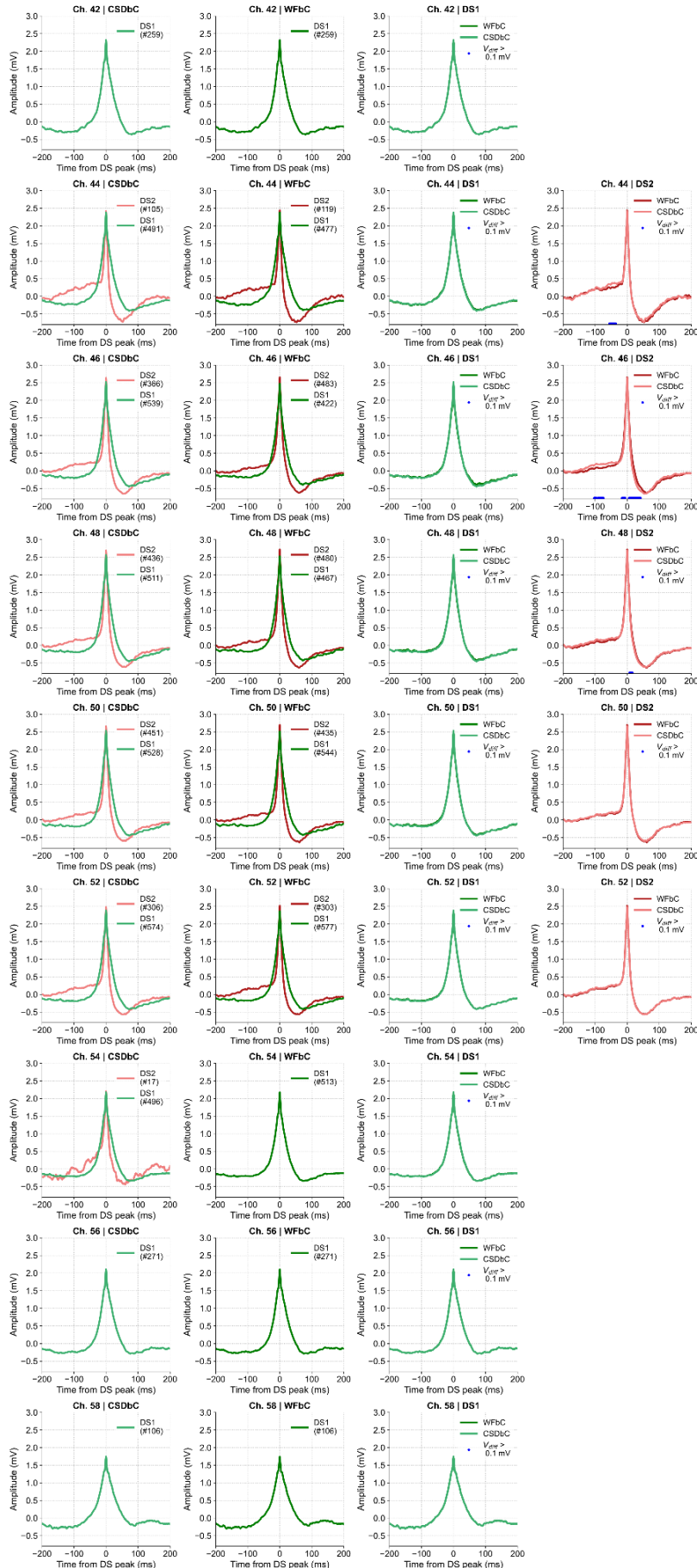


Figure S8. DS waveform comparison between methods for each channel of mouse B2.

The panels in the first and second columns show the waveforms of each DS type classified by CSDbC and WFbC respectively. The panels in the third and fourth columns compare the waveforms of DS1 and DS2 respectively. Each line represents the chosen channel for DS detection. CSD: current source density; CSDbC: CSD-based classification; DS: dentate spike; DS1: DS type 1; DS2: DS type 2; WFbC: waveform-based classification.

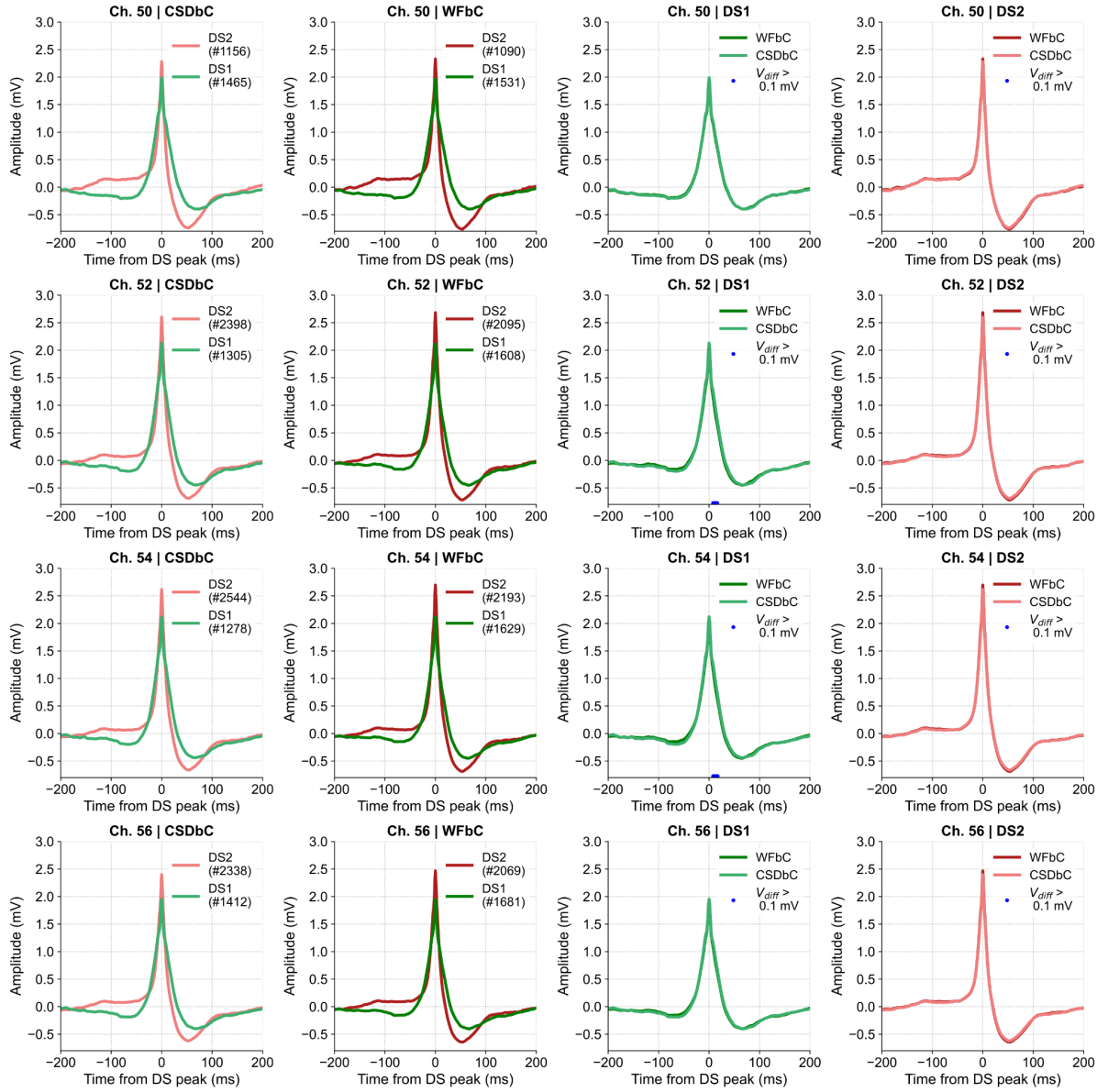


Figure S9. DS waveform comparison between methods for each channel of mouse B3.

The panels in the first and second columns show the waveforms of each DS type classified by CSDbC and WFbC respectively. The panels in the third and fourth columns compare the waveforms of DS1 and DS2 respectively. Each line represents the chosen channel for DS detection. CSD: current source density; CSDbC: CSD-based classification; DS: dentate spike; DS1: DS type 1; DS2: DS type 2; WFbC: waveform-based classification.

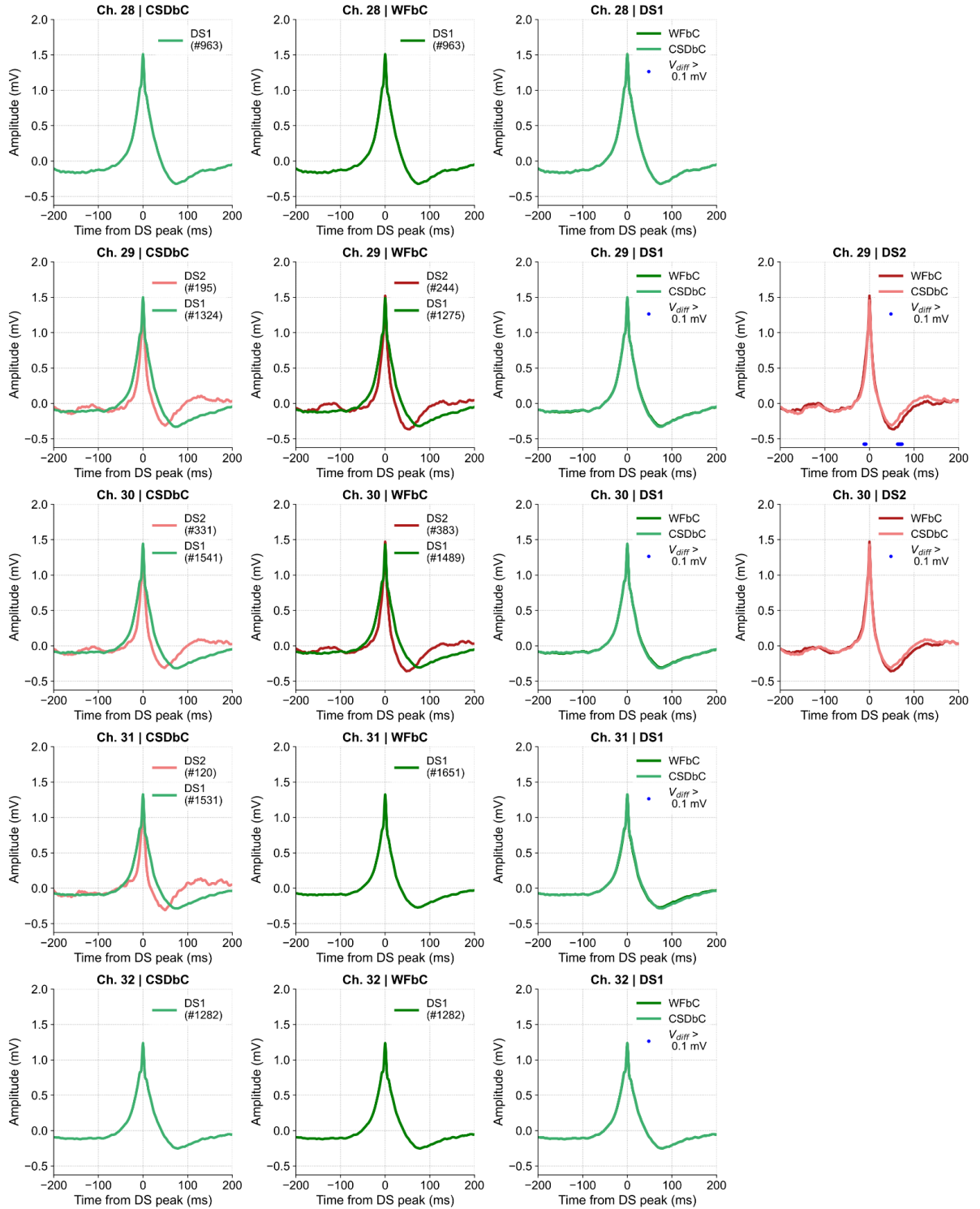


Figure S10. DS waveform comparison between methods for each channel of mouse C1.

The panels in the first and second columns show the waveforms of each DS type classified by CSDbC and WFbC respectively. The panels in the third and fourth columns compare the waveforms of DS1 and DS2 respectively. Each line represents the chosen channel for DS detection. CSD: current source density; CSDbC: CSD-based classification; DS: dentate spike; DS1: DS type 1; DS2: DS type 2; WFbC: waveform-based classification.

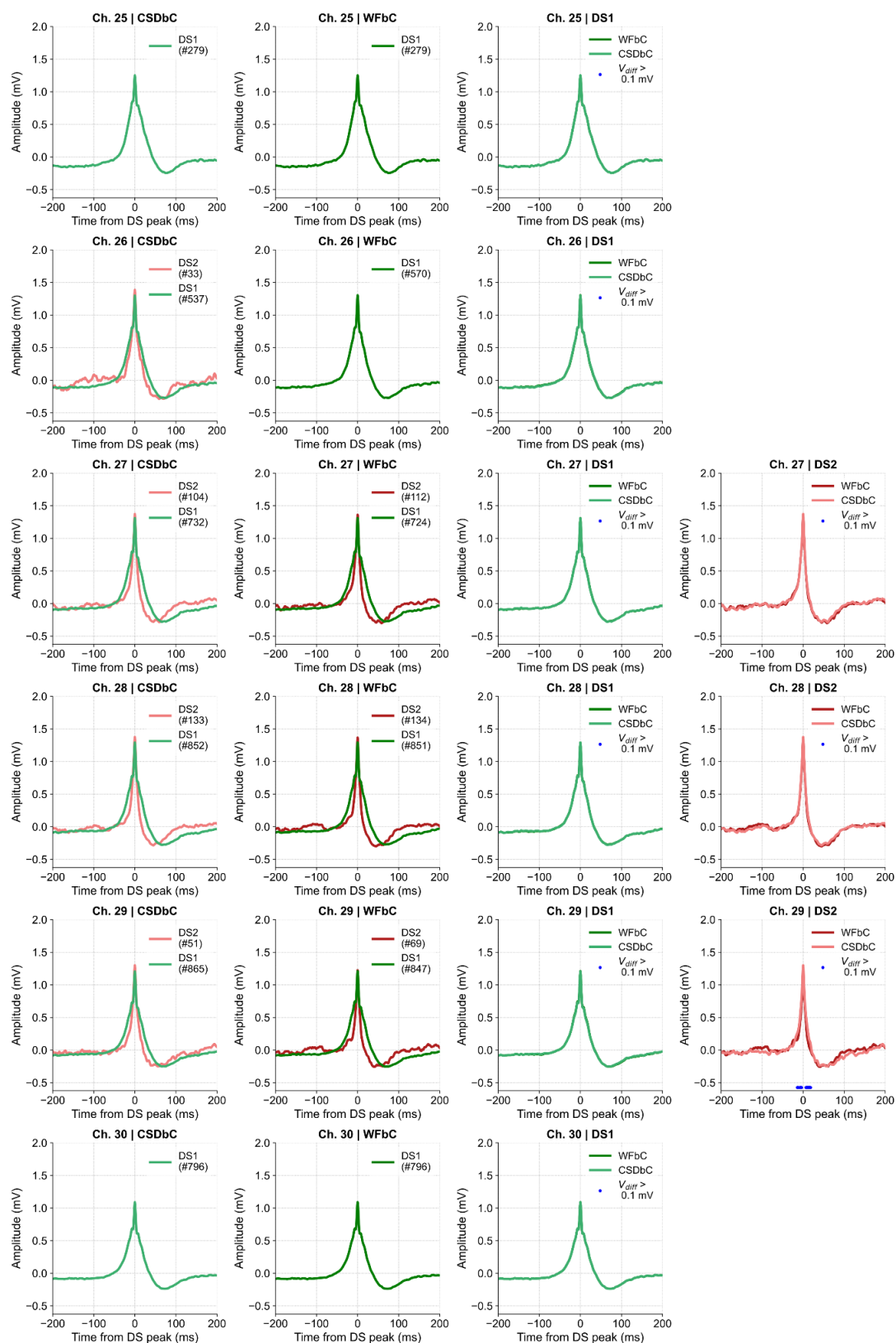


Figure S11. DS waveform comparison between methods for each channel of mouse C2.

The panels in the first and second columns show the waveforms of each DS type classified by CSDbC and WFbC respectively. The panels in the third and fourth columns compare the waveforms of DS1 and DS2 respectively. Each line represents the chosen channel for DS detection. CSD: current source density; CSDbC: CSD-based classification; DS: dentate spike; DS1: DS type 1; DS2: DS type 2; WFbC: waveform-based classification.

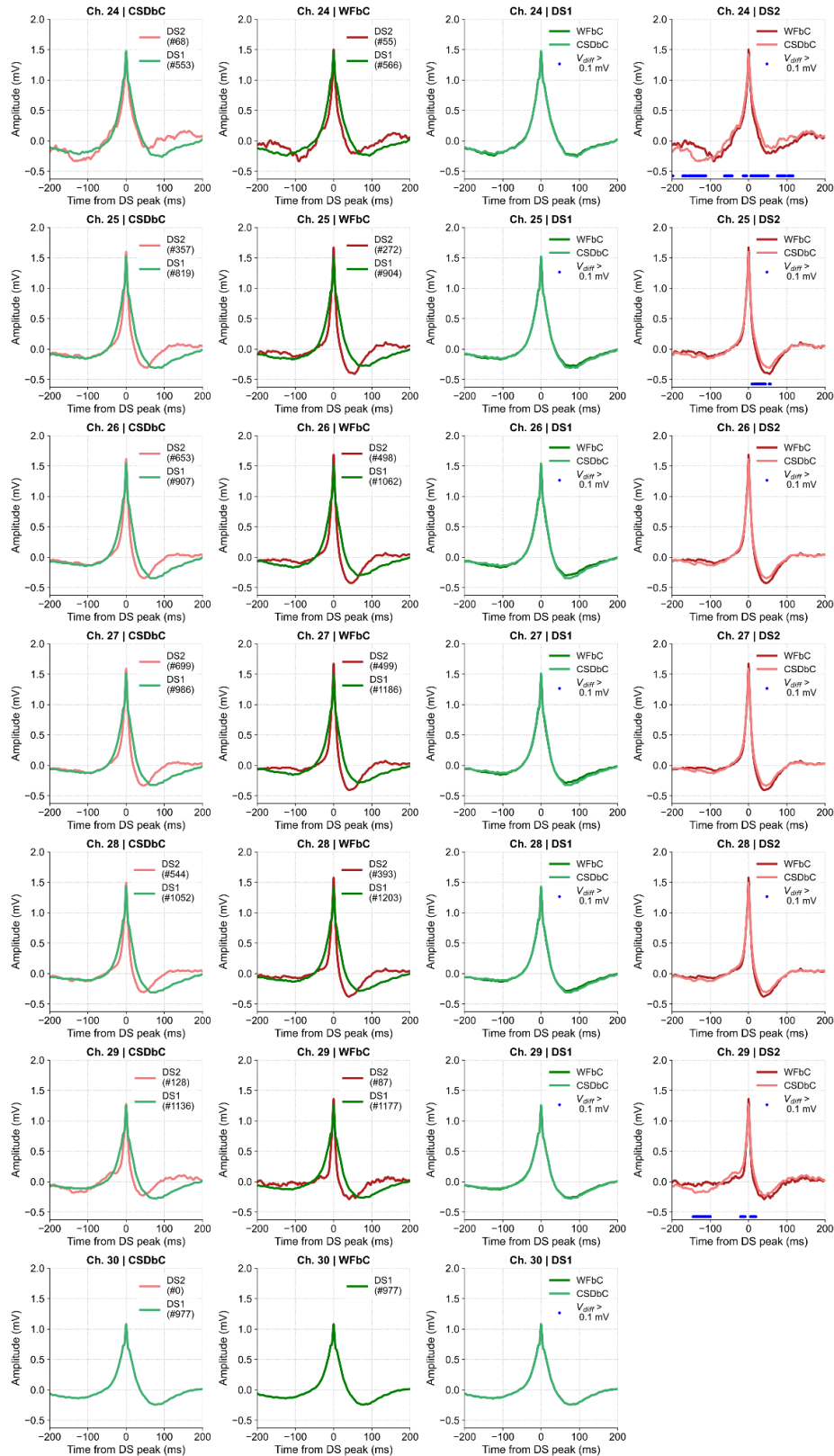


Figure S12. DS waveform comparison between methods for each channel of mouse C3.

The panels in the first and second columns show the waveforms of each DS type classified by CSDbC and WFbC respectively. The panels in the third and fourth columns compare the waveforms of DS1 and DS2 respectively. Each line represents the chosen channel for DS detection. CSD: current source density; CSDbC: CSD-based classification; DS: dentate spike; DS1: DS type 1; DS2: DS type 2; WFbC: waveform-based classification.

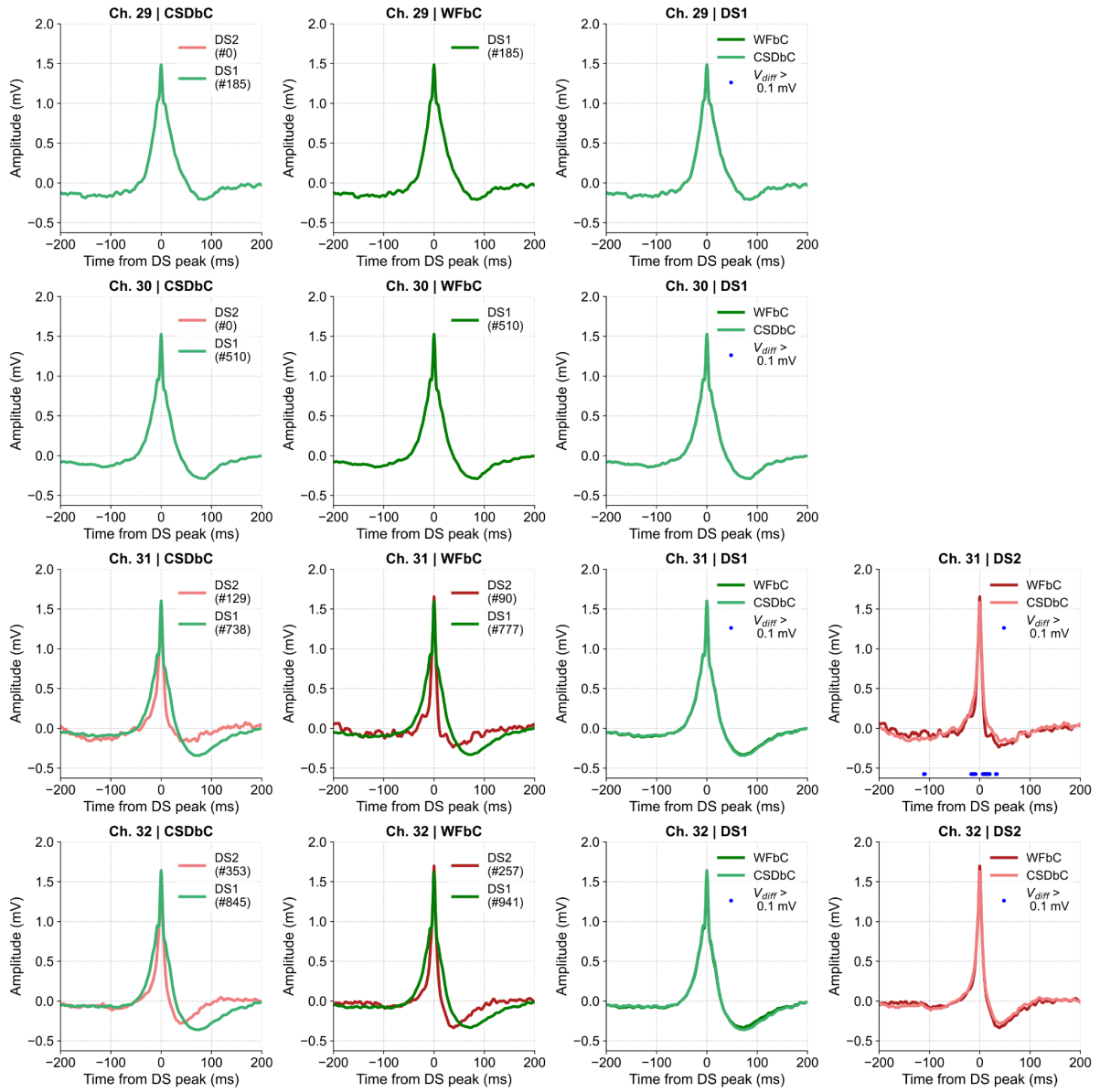


Figure S13. DS waveform comparison between methods for each channel of mouse C4.

The panels in the first and second columns show the waveforms of each DS type classified by CSDbC and WFbC respectively. The panels in the third and fourth columns compare the waveforms of DS1 and DS2 respectively. Each line represents the chosen channel for DS detection. CSD: current source density; CSDbC: CSD-based classification; DS: dentate spike; DS1: DS type 1; DS2: DS type 2; WFbC: waveform-based classification.

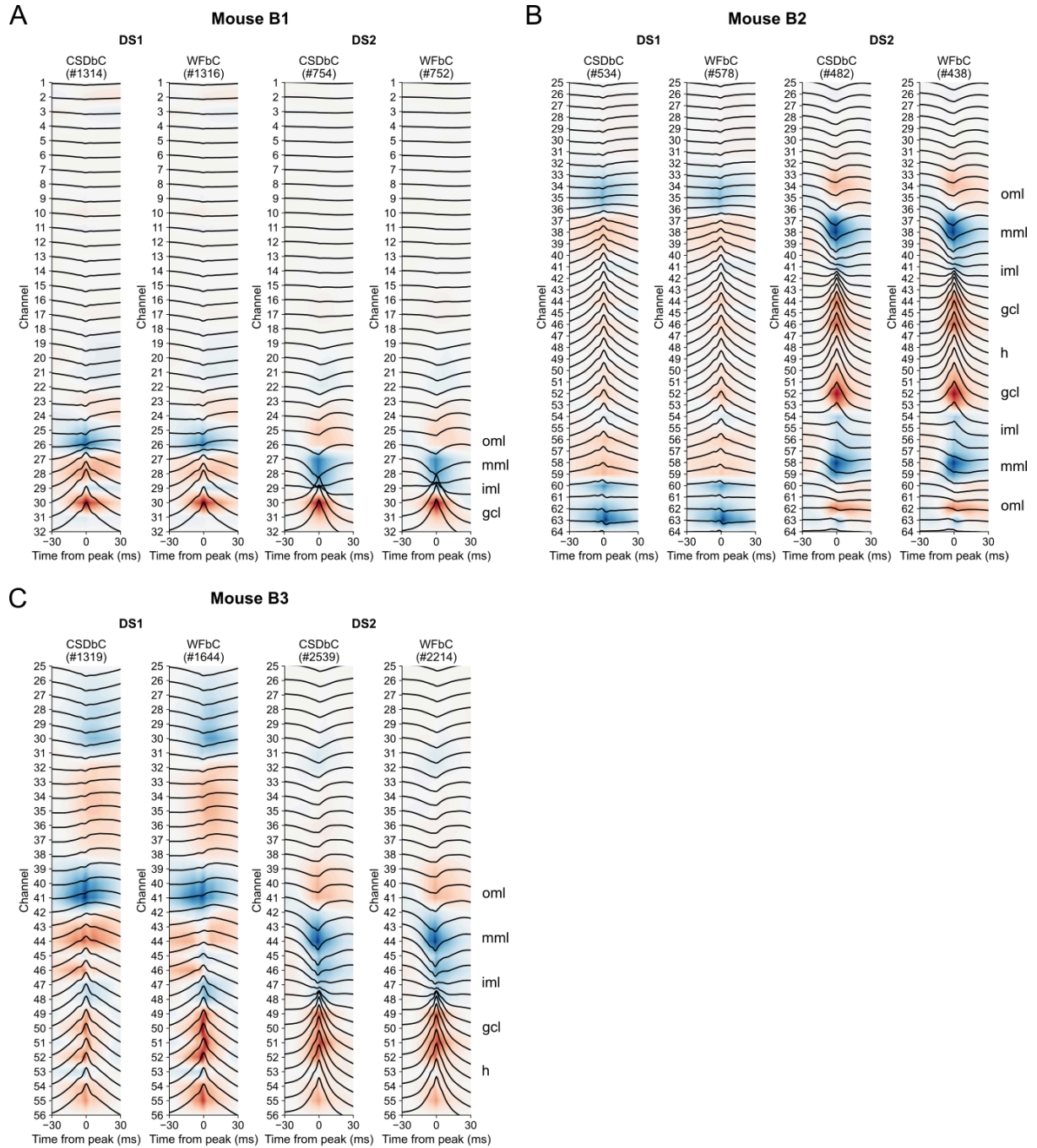


Figure S14. DS-triggered CSDs from mice of dataset B.

(A) Mean CSDs of mouse B1 within a 60-ms window around the peak of each DS type classified by CSDbC and WFbC. Blue and red colors represent sinks and sources, respectively. The estimated DG layers are indicated on the right. (B,C) Same as A, but for mice B2 and B3. CSD: current source density; CSDbC: CSD-based classification; DS: dentate spike; DS1: DS type 1; DS2: DS type 2; WFbC: waveform-based classification; gcl: granule cell layer; h: hilus; iml: inner molecular layer; mml: middle molecular layer; oml: outer molecular layer.

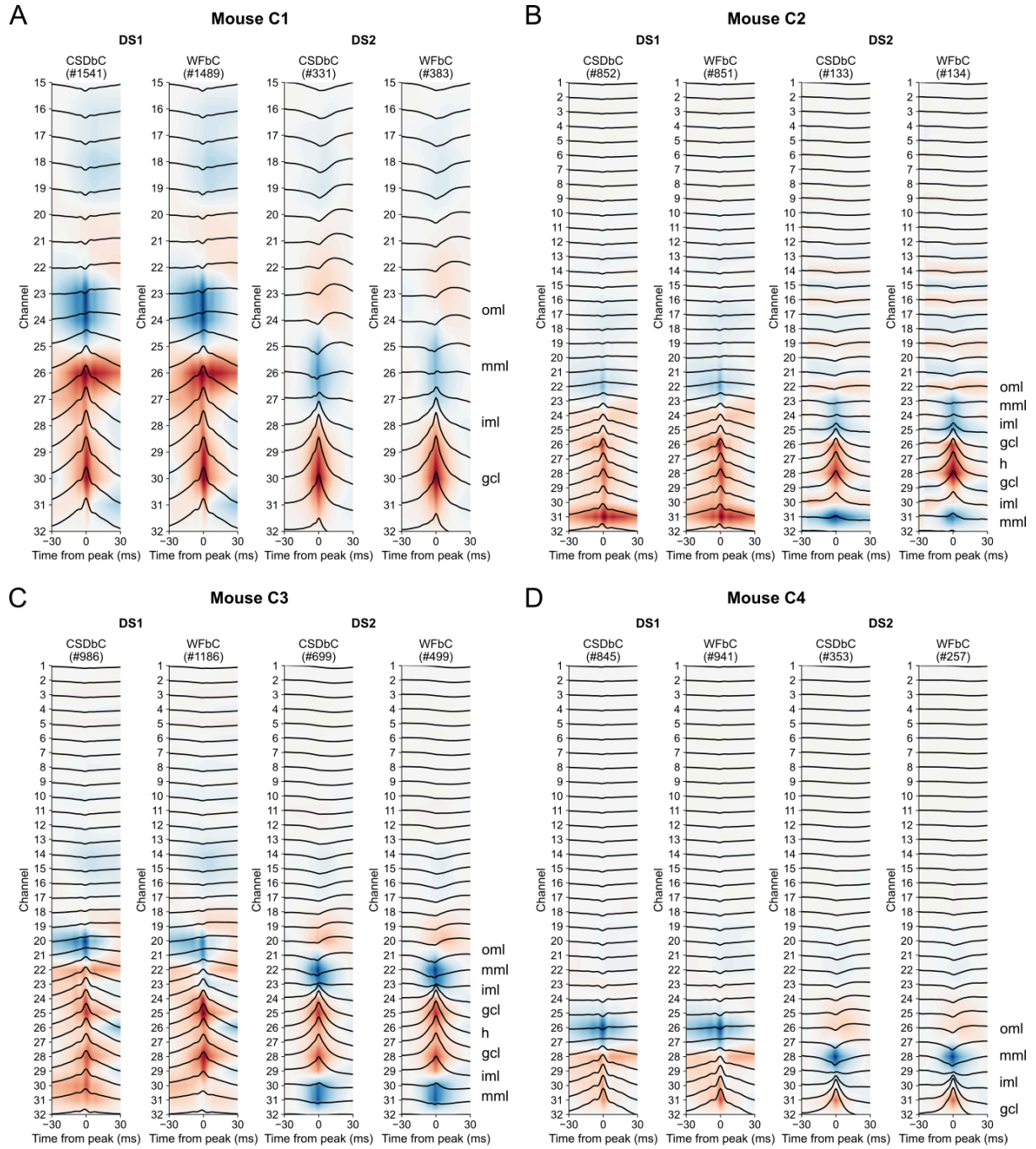


Figure S15. DS-triggered CSDs from mice of dataset C.

(A) Mean CSDs of mouse C1 within a 60-ms window around the peak of each DS type classified by CSDbC and WFbC. Blue and red colors represent sinks and sources, respectively. The estimated DG layers are indicated on the right. (B-D) Same as A, but for mice C2, C3 and C4. CSD: current source density; CSDbC: CSD-based classification; DS: dentate spike; DS1: DS type 1; DS2: DS type 2; WFbC: waveform-based classification; gcl: granule cell layer; h: hilus; iml: inner molecular layer; mml: middle molecular layer; oml: outer molecular layer.

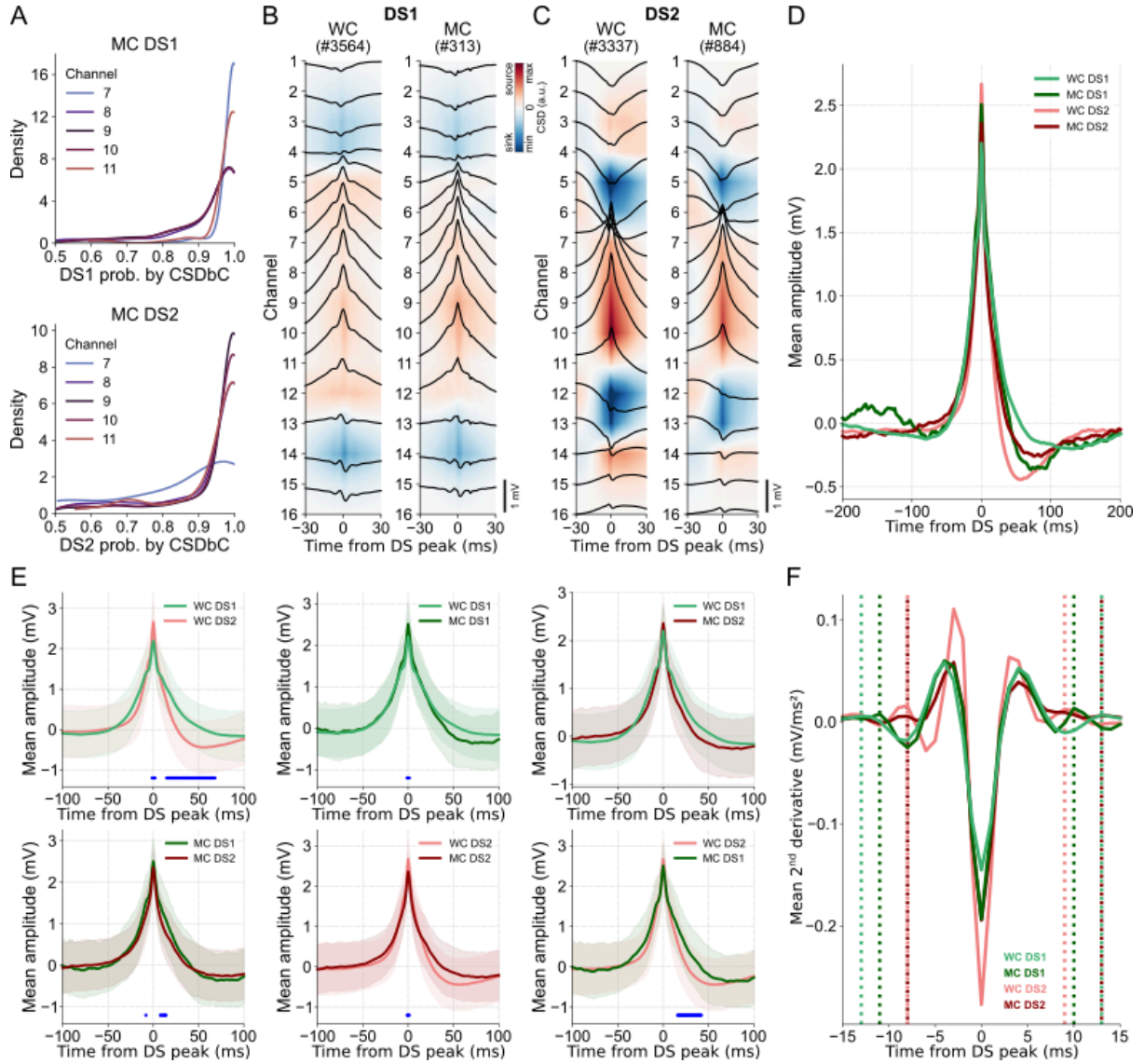


Figure S16. Misclassified DSs exhibit post-peak dynamics similar to related types.

(A) The probability densities of DS1 misclassified as DS2 by WFbC in channels 7 to 11 of mouse A is shown on top. The bottom panel shows the same for DS2. (B) Mean CSDs for the well-classified (left panel) and misclassified (right panel) DS1 by WFbC. (C) Same as B, but for DS2. (D) Mean waveforms of well- and misclassified DSs of both types in channel 9. (E) Pair-to-pair comparison of the waveforms shown in D. The blue dots indicate when Cohen's D size effect is greater than 0.5 for periods with significant differences ($p < 0.05$ in t-test) between the waveforms. (F) Mean 2nd derivatives of the waveforms shown in D. The dotted lines indicate the start and end width limits of each waveform. DS1: dentate spike type 1; DS2: dentate spike type 2; MC: misclassified; WC: well-classified.

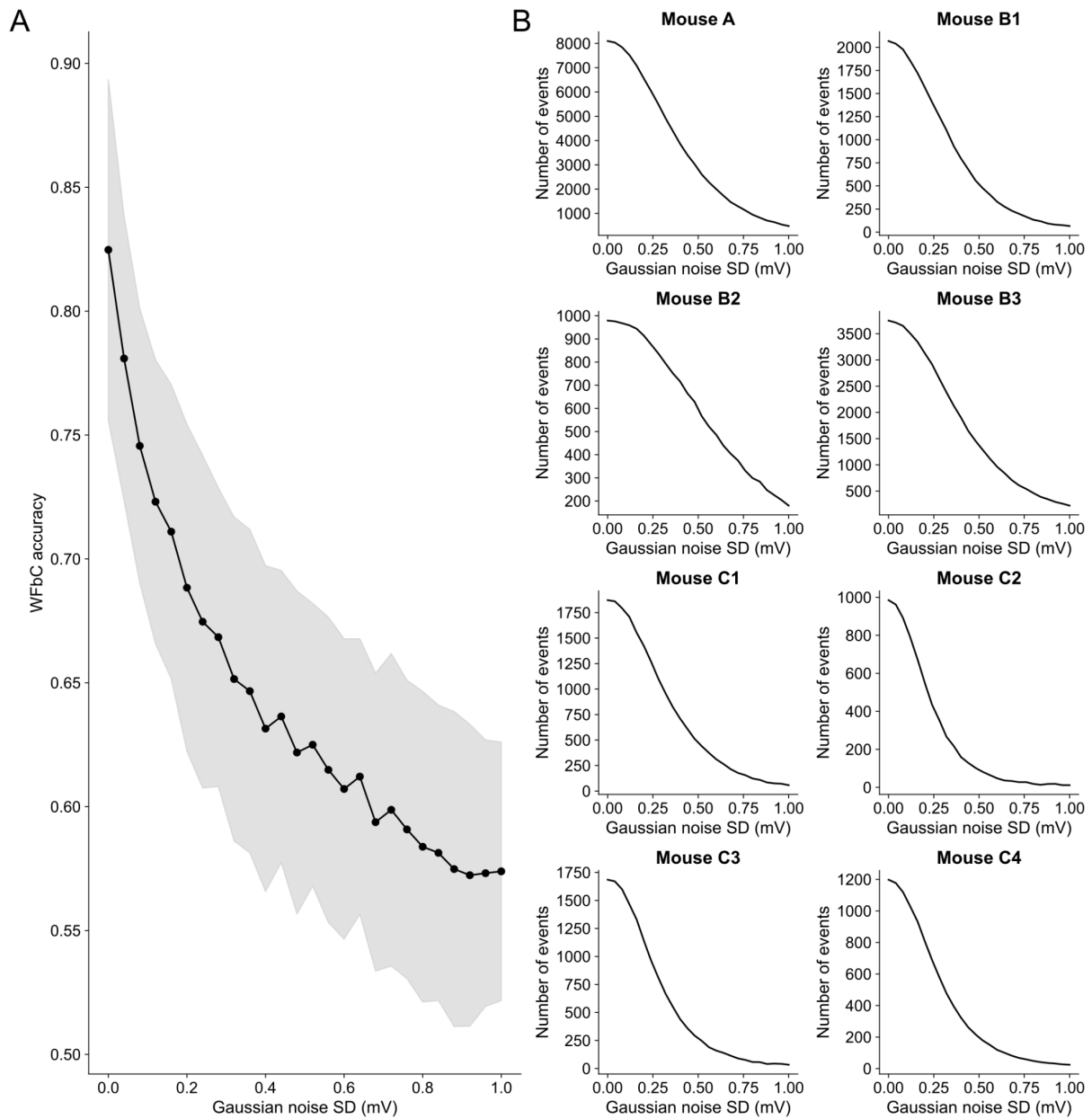


Figure S17. Effect of Gaussian noise on WFbC performance and DS detection.

(A) WFbC accuracy in function of the noise intensity. The latter corresponds to the standard deviation of the Gaussian noise distribution (zero mean), which was added to the waveforms of the DSs after their detection on the hilus channels and classification via CSDbC. The events were distributed equally between DS1 and DS2 (50% each) before WFbC classification. For each noise level, the black dot indicates the mean accuracy across animals for 20 different noise runs; the gray shadow indicates the standard deviation. (B) Each panel shows the number of events detected as DSs in function of the standard deviation of the Gaussian noise added to the hilar LFP of each animal. SD: standard deviation; WFbC: waveform-based classification.

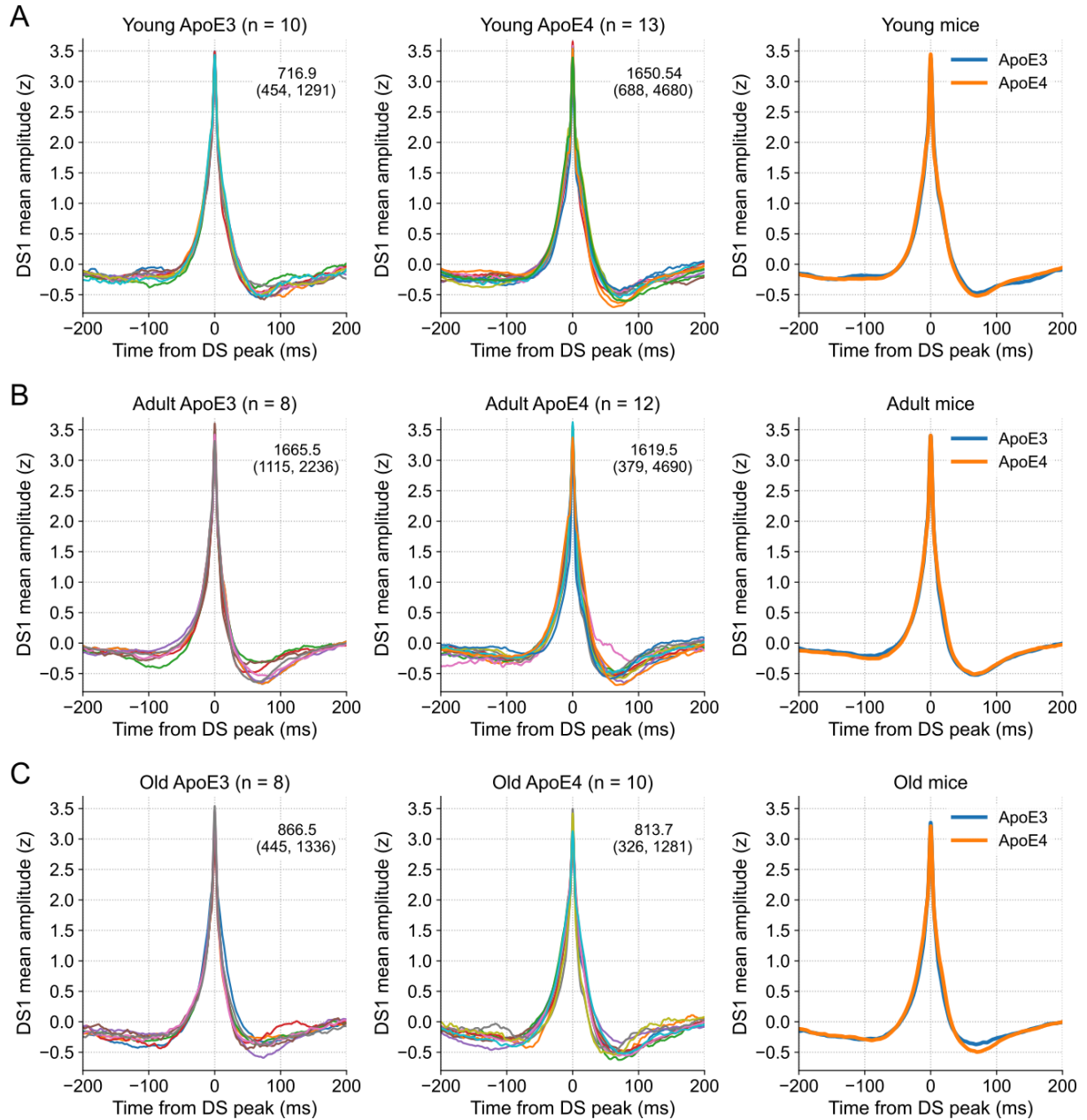


Figure S18. DS1 mean waveforms of ApoE3-KI and ApoE4-KI mice.

(A) DS1 mean waveforms of each ApoE3-KI mouse (left panel) and each ApoE4-KI mouse (middle panel) when young. Numbers within the graphs indicate the average number of events with minimum and maximum values in parentheses. The comparison of overall mean waveforms is shown in the right panel. (B,C) Same as A, but for mice in adult and old ages. ApoE3-KI: Apolipoprotein E3 knock-in mice; ApoE4-KI: Apolipoprotein E4 knock-in mice; DS1: dentate spike type 1; DS2: dentate spike type 2.

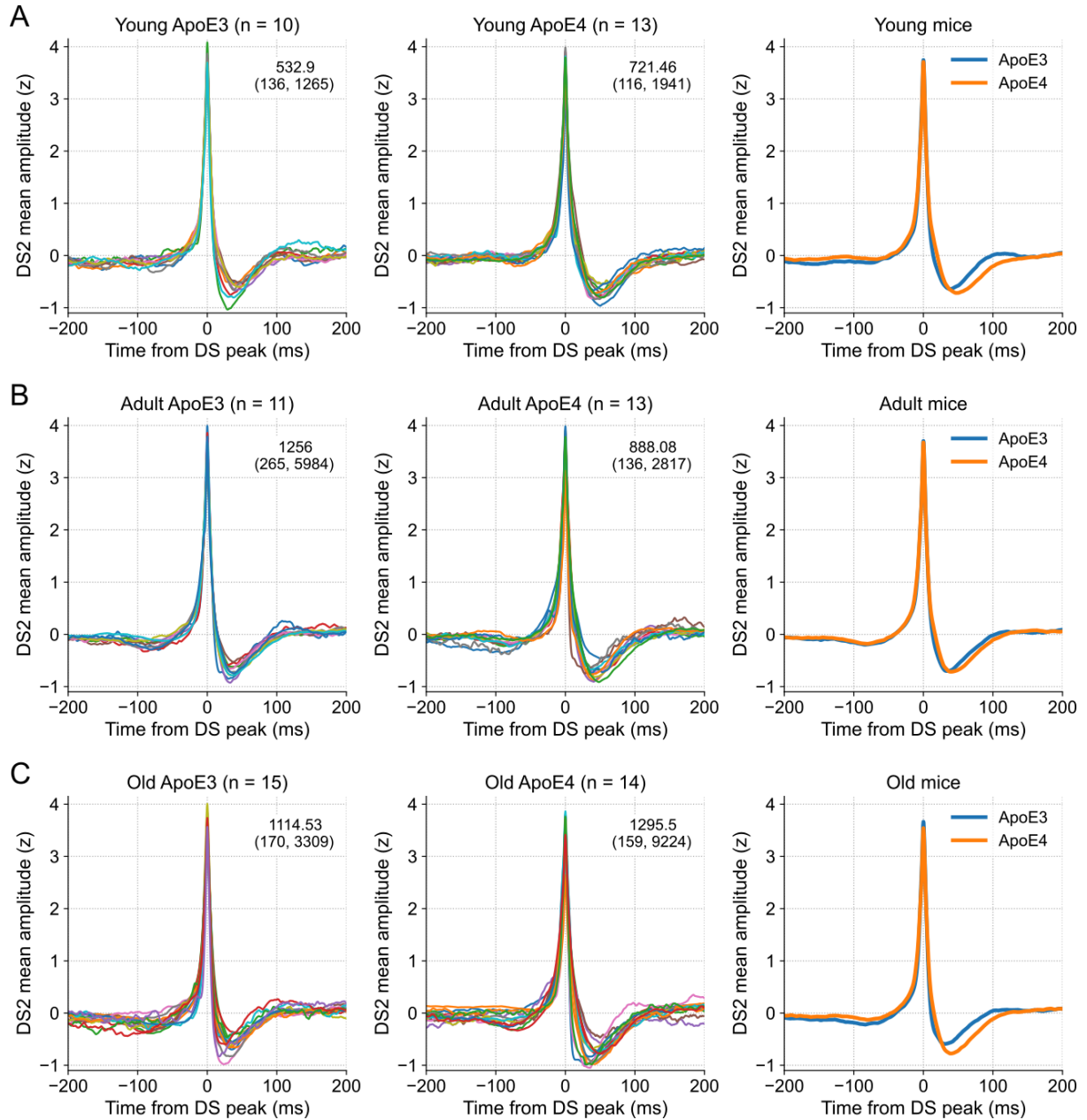


Figure S19. DS2 mean waveforms of ApoE3-KI and ApoE4-KI mice.

(A) DS2 mean waveforms of each ApoE3-KI mouse (left panel) and each ApoE4-KI mouse (middle panel) when young. Numbers within the graphs indicate the average number of events with minimum and maximum values in parentheses. The comparison of overall mean waveforms is shown in the right panel. (B,C) Same as A, but for mice in adult and old ages. ApoE3-KI: Apolipoprotein E3 knock-in mice; ApoE4-KI: Apolipoprotein E4 knock-in mice; DS1: dentate spike type 1; DS2: dentate spike type 2.

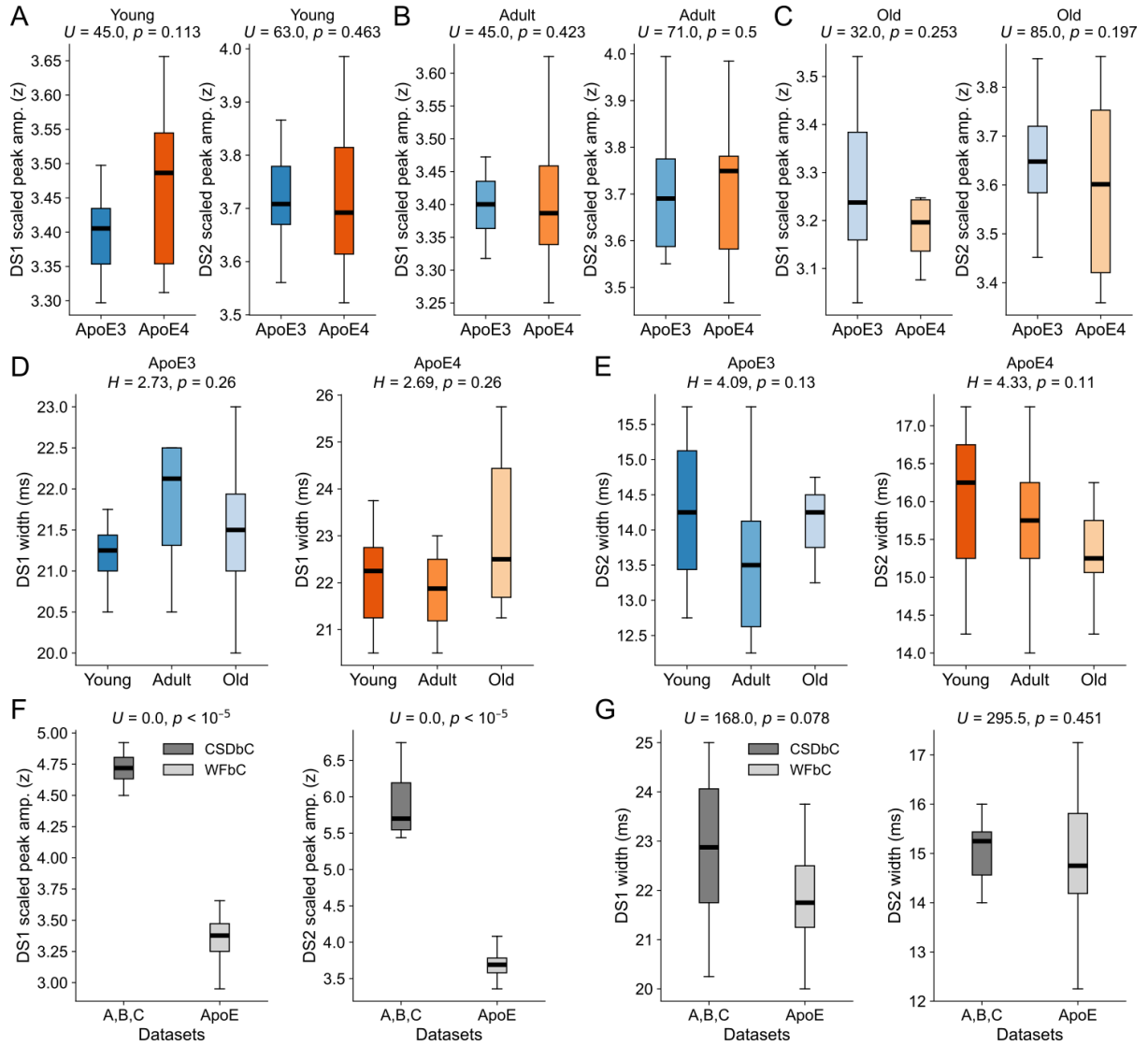


Figure S20. Stable DS metrics across genotypes, ages and datasets.

(A) Comparison of the scaled peak amplitudes of DS1 (left panel) and DS2 (right panel) between young ApoE3-KI and ApoE4-KI mice. (B,C) Same as A, but for mice in adult and old ages. (D) Comparison of DS1 widths of ApoE3-KI (left panel) and ApoE4-KI mice (right panel) across ages. (E) Same as D, but for DS2. (F) Comparison of scaled peak amplitudes of DS1 (left panel) and DS2 (right panel) between mice from datasets A-B-C and ApoE transgenic mice, whose DSs were classified via CSDbC and WFbC respectively. (G) Same as F, but for DS widths. Statistics and p -values were obtained from Mann-Whitney U tests for panels in A-C,F,G, and from Kruskal-Wallis H tests for panels in D and E. ApoE3-KI: Apolipoprotein E3 knock-in mice; ApoE4-KI: Apolipoprotein E4 knock-in mice; DS1: dentate spike type 1; DS2: dentate spike type 2.

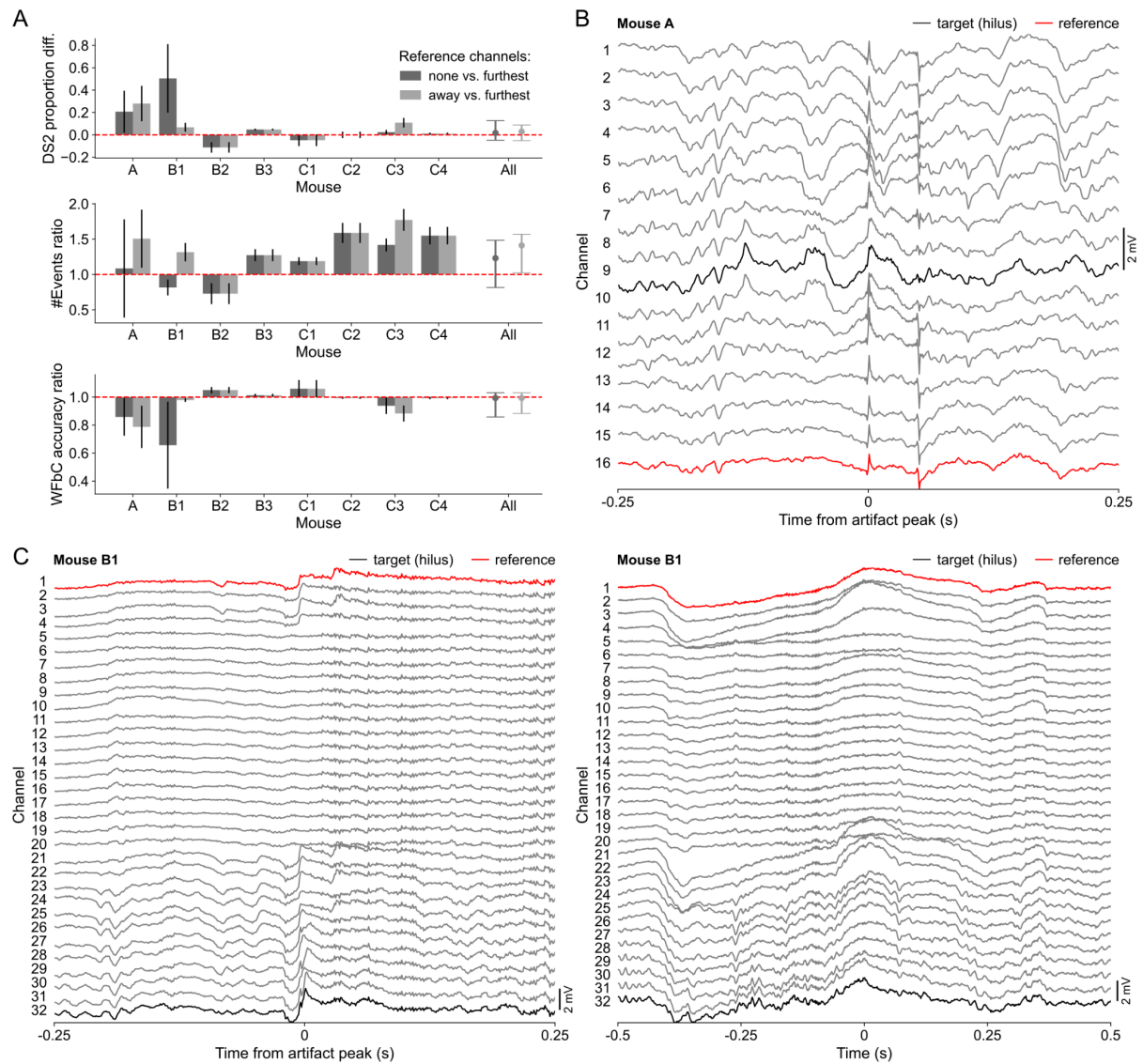


Figure S21. Analysis of the choice of the reference signal used to avoid the detection of artifacts as DSs. (A) The top panel shows the differences in the DS2 proportions returned by CSDbC when using alternative reference subtraction procedures for artifact mitigation when detecting DSs. The dark gray bars compare the use of no reference channel with the use of the furthest channel from the hilus (i.e., the standard method employed in our study). The light gray bars compare the use of the mean LFP of the channels away from hilus (from OML onwards) as the reference signal vs. the standard method. The mean (bar) and standard deviation across the relevant channels are shown for each animal. The median (dot) across animals and its 95% confidence interval are shown on the right. The red dashed line corresponds to no differences. The middle and bottom panels show the same, but for the ratios of the number of detected events between the procedures and the ratios of the Wfbc accuracies. (B) Example of the most common artifact type observed in mouse A. Its detection as DS was avoided by subtracting the LFP of the reference channel (red) from the LFP of the target channel (black). (C) Same as B, but for the two most common types of artifacts observed in mouse B1. In contrast to mouse A, where all channels were affected, the artifacts from mouse B1 only impacted the first 4 and last 12 channels.

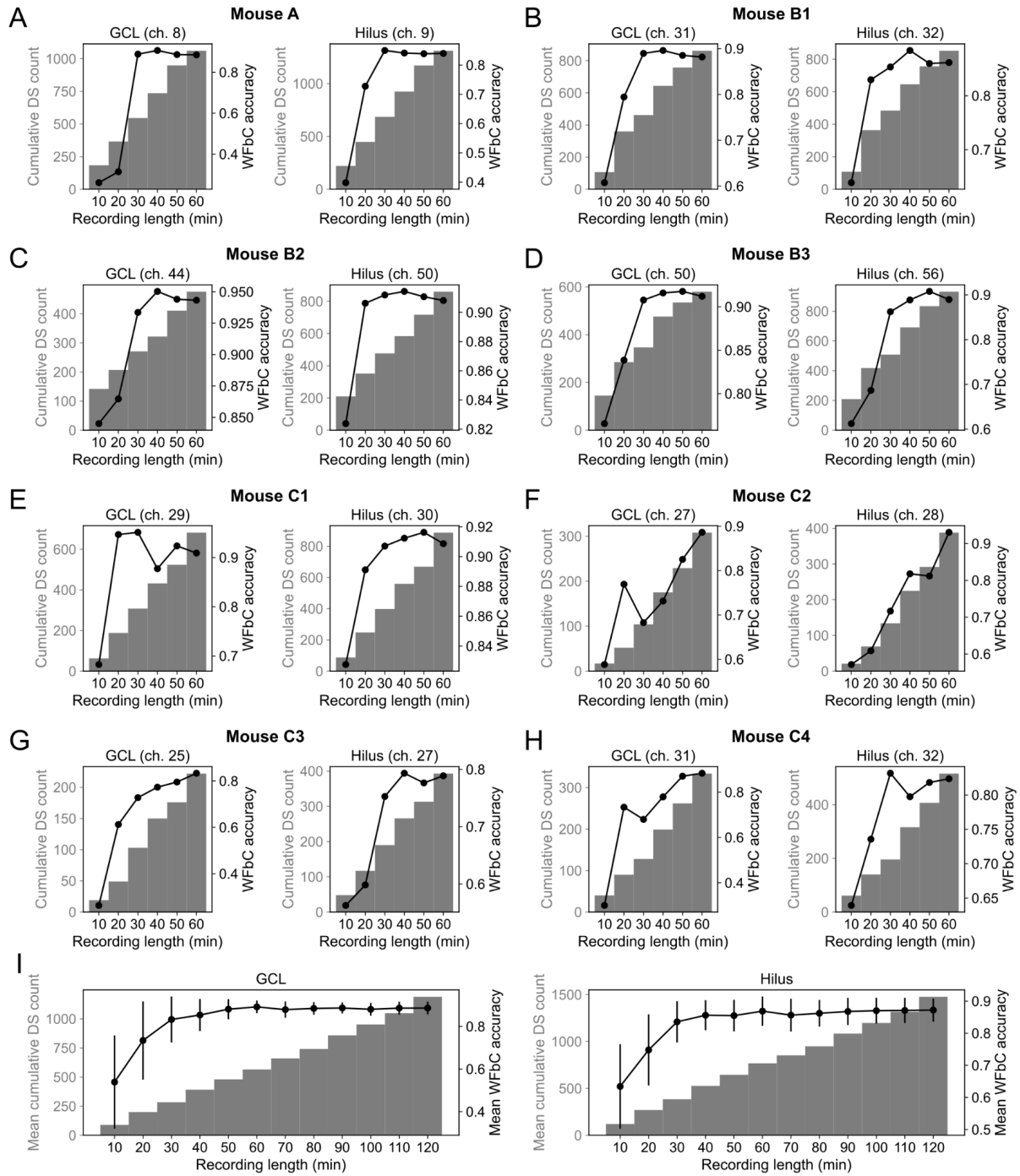


Figure S22. WFbC accuracy in function of the recording length.

(A) Cumulative DS count (gray bars) and WFbC accuracy (black dots) related to the recording length for GCL (left panel) and hilus (right panel) LFPs of mouse A. Data from sleep/rest periods with high delta power were concatenated. (B-H) Same as A, but for mice B1-3 and C1-4. (I) Same as A, but for the mean values across all mice. Black error bars indicate standard deviations. DS: dentate spike; GCL: granule cell layer.